Check for updates

High-valent oxovanadium metallosupramolecular species as catalysts for the oxidation of benzyl alcohol derivatives†

Edi Topić, [ID] [a] Josipa Sarjanović, [ID] [a] Danijela Musija, [ID] [b] Mirna Mandarić, [ID] [a] Tomica Hrenar, [ID] [a] Jana Pisk [ID] *[a] and Višnja Vrdoljak [ID] *[a]

Coordination-driven synthesis has been successfully utilized to prepare vanadium-based metallosupramolecular species. By systematically varying synthesis methods and reaction conditions, two series of isostructural oxovanadium(v) coordination polymers $[VO(SIH)(OR)]_n$ (where SIH^{2-} represents salicylaldehyde isonicotinoylhydrazonate, and R corresponds to CH_3 (**1β**·0.25CH$_3$OH), C_2H_5 (**2α** and **2β**·0.25C$_2$H$_5$OH), C_3H_7 (**3α**), C_4H_9 (**4α** and **4β**), and C_5H_{11} (**5β**)), were synthesized. Additionally, a phase-pure tetranuclear compound $[VO(SIH)(OCH_3)]_4$·4CH$_3$OH (**1t**·4CH$_3$OH) was also prepared. In these compounds the [VO(SIH)] units, featuring the isonicotinoylhydrazonate heterocyclic moiety, are interconnected through V–N$_{isonicotinoyl}$ coordination bonds. This linkage enables formation of the one-dimensional (1D) zig–zag chain compounds and zero-dimensional (0D) metallocycle, as determined by single crystal X-ray crystallography. This study further explored the formation and transformation of the assemblies, thereby emphasizing the influence of the ancillary OR$^-$ ligand. The compounds were also characterized by powder X-ray diffraction, chemical analysis, thermogravimetric (TGA) measurements, and spectroscopic methods (IR-ATR, UV-Vis, and NMR). The catalytic activity of vanadium coordination entities **1t** and **1β** was tested for the oxidation of benzyl alcohol and its derivatives, including 2-nitrobenzyl, 2-chlorobenzyl, and 2-methylbenzyl alcohol. Several oxidizing agents were used, including *tert*-butyl hydroperoxide (TBHP) in aqueous and decane solutions, as well as hydrogen peroxide (H$_2$O$_2$). The study also assessed the impact of different solvents, such as toluene, acetonitrile, and methanol, thereby enhancing the understanding of these systems.

Introduction

High-valent metal–organic species are widely recognized as active oxidants in the catalytic oxidation of organic compounds, serving as a cornerstone in both academic research and industrial applications.[1–4] Their utilization requires careful consideration of several factors to optimize performance and efficiency. These factors include not only the selection of the central metal but also the choice and variation of ligands. Ligand substituents significantly influence the solubility,

[a]University of Zagreb, Faculty of Science, Department of Chemistry, Horvatovac 102a, 10000 Zagreb, Croatia. E-mail: jana.pisk@chem.pmf.hr; visnja.vrdoljak@chem.pmf.hr

[b]University of Zagreb, School of Medicine, Department of Chemistry and Biochemistry, Šalata 3, 10000 Zagreb, Croatia

† Electronic supplementary information (ESI) available: (1) Powder diffraction patterns, (2) additional figures for compounds, (3) tables of selected bond distances and angles and of hydrogen bonds parameter, (4) UV-Vis spectra, (5) NMR spectra ATR-IR spectra, (6) TGA curves, (7) crystallographic data sets for the structures **1t**·4CH$_3$OH, **2α**, **3α**, **4α**, **1β**·0.25CH$_3$OH, **2β**·0.25C$_2$H$_5$OH and **5β**. CCDC 2367532–2367538. For ESI and crystallographic data in CIF or other electronic format see DOI: https://doi.org/10.1039/d4ra09073j

stability, electronic structure, and steric properties of the complex system, all of which ultimately affect catalyst performance.

Among these systems, oxovanadium complexes are particularly notable due to the advantageous characteristics of the vanadium metal center.[5–7] Vanadium exhibits a variety of oxidation states, different coordination numbers, enhanced oxophilicity, and a good Lewis acidity.[8,9] These properties make vanadium-based catalysts highly effective in promoting the oxidation of organic substrates, including saturated, aromatic, and olefinic hydrocarbons.[10–12] Despite these advantages, the development and application of high-valent oxovanadium metallosupramolecular compounds as catalysts remain relatively underexplored. High-valent vanadium complexes tend to form oxo- or alkoxo-bridged compounds, limiting their use in creating well-defined supramolecular structures.[13–15] To the best of our knowledge, there are only rare examples of VO coordination polymers or cyclic assemblies $[VO(L)(L')]_x$ (L, L' = ligands) comprising nitrogen and oxygen donor ligands.[16–20]

In contrast, significant progress in this area has been made for high-valent metallosupramolecular species, such as molybdenum(vi) and tungsten(vi) assemblies bearing terminal oxo co-

ligands.[21–25] These species are synthesized using carefully designed organic ligands and strict control of the reaction conditions, preventing oligomerization of the highly reactive metal-oxo units through the oxygen atom.[21–24] The size, shape of these assemblies, and the functional groups of all building units are also essential and determine their properties and potential application.[25,26]

From a structural perspective, one could anticipate observations of multiple crystal forms for the same metallosupramolecular assembly, however, polymorphism in metal–organic chemistry is seldom reported on; less than 0.5% of metal–organic structures in the Cambridge Structural Database have corresponding polymorphs. Moreover, the occurrence of polymorphism is unevenly distributed, particularly among first-row transition metals. Among these, iron and copper compounds exhibit the highest frequency of polymorph occurrence, aligning with their abundant entries in the database. Vanadium compounds, however, stand out as an exception compared to their periodic table neighbours, displaying a relatively high number of polymorphs compared to the total number of published crystal structures (Fig. 1).

Focusing on neutral vanadium complexes, a few studies have reported polymorphs of vanadium(III), oxovanadium(IV), (alkoxo)oxovanadium(V), and dioxovanadium(V) species. These polymorphs are associated with a variety of ligands, including pyridine derivatives,[27,28] Schiff bases,[29–31] hydrazones, and related compounds.[32–36] Additionally, polymorphism has been observed in heteropolymetallic coordination polymers containing dioxovanadium(V) ions[37,38] and vanadium complexes with porphyrin derivatives.[39–41] Interestingly, polymorphism is predominantly found in compounds lacking strong directional intermolecular interactions, such as hydrogen or halogen

bonding. This suggests that vanadium compounds are prone to polymorphism in the absence of significant supramolecular synthons. However, this observation also implies that incorporating well-defined supramolecular synthons in the ligand design might hinder exploration of the polymorphic landscape.

Despite these findings, the structural chemistry of vanadium remains relatively underexplored compared to other transition metal complexes. Consequently, these insights should be regarded as preliminary rather than definitive, until more structural data is collected.

Although constructing metallosupramolecular architectures with oxovanadium(V) building blocks is more challenging, the potential of these types of compounds is highly promising and worth exploring.[42] In this study, we therefore explored their synthesis by employing a coordination-driven self-assembly methodology as an effective tool for constructing discrete or polynuclear architectures.[43–47] The [VO(SIH)] structural unit, incorporating the salicylaldehyde isonicotinoylhydrazonate ligand (SIH^{2-}) has been selected since the ligand features a heterocyclic moiety that provides a coordinating platform with a nitrogen donor atom. The choice of this ligand without additional substituents ensures that neither electron donating nor electron withdrawing groups interfere with the formation of the desired superstructures. In the presence of primary alcohols ROH ($C_nH_{2n+1}OH$, $n = 1–5$) building units can combine and yield metallocyclic $[VO(SIH)(OR)]_4$ or polymeric assemblies $[VO(SIH)(OR)]_n$. We also explored transformation of the assemblies by alkoxo OR^- ligand exchange.

By changing synthesis method and reaction conditions, two series of isostructural polymorphs were obtained (where R = CH_3 (**1β**·0.25CH_3OH), C_2H_5 (**2α** and **2β**·0.25C_2H_5OH), C_3H_7 (**3α**), C_4H_9 (**4α** and **4β**), and C_5H_{11} (**5β**)). The structures of these
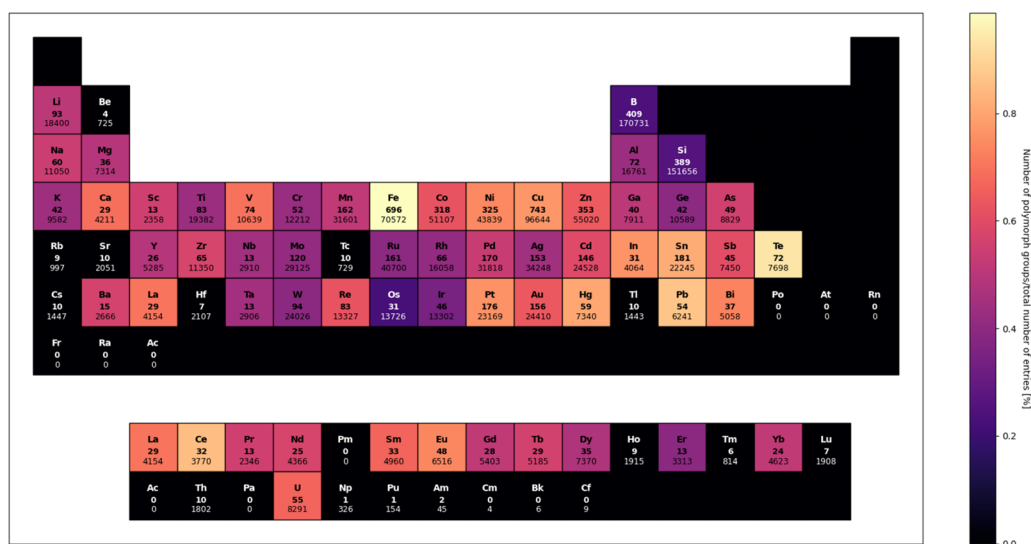

Fig. 1 Periodic table of polymorph occurrence among crystal structures containing metal or semi-metal elements in Cambridge Structural Database. Polymorph group was defined as set of structures with the same refcode root and distances between reduced unit cell vectors of at least 0.5. Number in bold font represents number of polymorph groups (*i.e.* groups of crystal structures with same composition and molecular structure, but different unit cell or packing of molecules). Number in regular font represents total number of entries containing a particular element. Colour of element box (1) maps normalized polymorph occurrence or (2) is black if number of found polymorph groups is less or equal to 10.

oxovanadium(v) polymers and metallocyclic compound [VO(SIH)(OCH₃)]₄·4CH₃OH (**1t**·4CH₃OH), were elucidated using single-crystal X-ray diffraction (SCXRD) and powder X-ray diffraction (PXRD) analysis. They were further characterized using elemental analysis, infrared (IR-ATR), UV-Vis, and NMR spectroscopic methods. The thermal stability of the assembled structures was also studied using thermogravimetric analysis (TGA).

These above mentioned findings suggest that similar strategies could be employed to advance the field of high-valent oxovanadium catalysts, opening new avenues for the development of efficient and selective oxidation processes. Due to it, we chose to investigate the oxidation of benzyl alcohol as it is extensively used as a precursor in the synthesis of various products.[48,49] Common oxidizing agents for the oxidation processes, potassium permanganate and sodium dichromate, are causing environmental issues.[50] While nitric acid is another commonly used and cost-effective oxidant its use leads to the formation of side products that are both toxic and environmentally polluting. Environmentally acceptable oxidants would be hydrogen peroxide or molecular oxygen which were tested for benzaldehyde oxidation assisted by transition metals such as Co, Fe, Sn–W, V and Au.[51–56]

Our research was focused on the catalytic performance of V-coordination entities **1t** and **1β** whose activity was compared to the compounds [VO₂(HSIH)] (**6**), V₂O₅, and [MoO₂(SIH)]ₙ.[57] They were assessed in oxidizing benzyl alcohol and its derivatives: 2-nitrobenzyl, 2-chlorobenzyl, and 2-methylbenzyl alcohol. The oxidation of benzyl alcohol derivatives to the corresponding carbonyl compounds was explored using various oxidizing

agents, including *tert*-butyl hydroperoxide (TBHP) in aqueous and decane solutions, as well as hydrogen peroxide (H₂O₂), while also evaluating the influence of different solvents such as toluene, acetonitrile, and methanol.
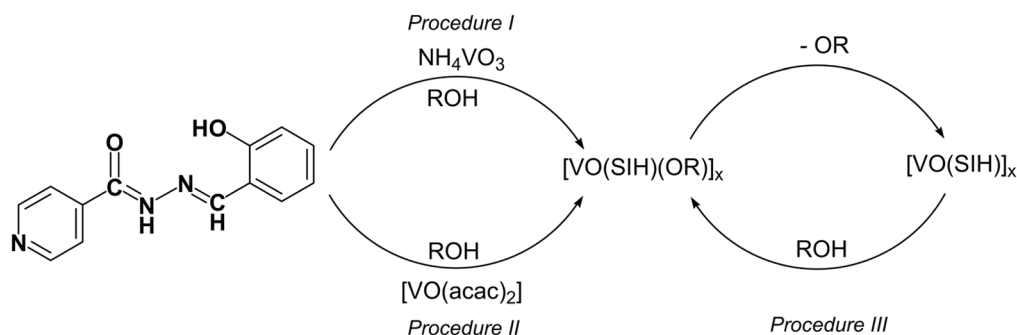
Results and discussion

Synthesis and characterization of metallocycle and two series of coordination polymers

The hydrazone derived from salicylaldehyde and iso-nicotinoylhydrazide was synthesized as described in the literature.[58] Supramolecular coordination complexes were afforded through the reaction of NH₄VO₃ or [VO(acac)₂], hydrazone (H₂SIH), and the corresponding primary alcohol (CₙH₂ₙ₊₁OH, n = 1–5) (Table 1, Scheme 1, Procedures I and II). The solvent was evaporated leaving a dark red coloured solution from which a crystalline precipitate formed. All compounds were characterized using various analytical and spectroscopic methods and were identified as tetranuclear metallocyclic [VO(SIH)(OCH₃)]₄·4CH₃OH (**1t**·4CH₃OH), and infinite zig–zag chain products [VO(SIH)(OR)]ₙ (where R = CH₃ (**1β**·0.25CH₃-OH), C₂H₅ (**2α** and **2β**·0.25C₂H₅OH), C₃H₇ (**3α**), C₄H₉ (**4α** and **4β**), and C₅H₁₁ (**5β**), Table 1). Their formation was driven by the denticity of the ligand and donor atom positions within the linking unit. The crystalline powders were analysed using PXRD and the results were then compared to the simulated powder patterns obtained from the SCXRD data (Fig. S1–S3, see ESI†). In the case of polynuclear assemblies, two series of polymorphic forms were characterized. The structures of **2α**, **3α**, and **4α** belong to the first arrangement (Fig. S2†), while the structures of **1β**·0.25CH₃OH, **2β**·0.25CH₃OH, **4β**, and **5β** belong to the second one (Fig. S3†). The observed similarities in the powder diffractograms within each series facilitate the determination of the polymorphic type associated for each compound. Despite our attempts, we didn't obtain **1α**, **3β**, and **5α** forms by the mentioned procedures. Following Procedure I, **4β** polymorph can be isolated upon the evaporation of the reaction solution on the same day. In contrast, the **4α** form is generated when the solution remains undisturbed for an extended period.

Furthermore, by immersing crystals of the tetramer [VO(SIH)(OCH₃)]₄·4CH₃OH (**1t**·4CH₃OH) in an appropriate coordinating solvents ROH (R = CₙH₂ₙ₊₁, n = 2–5), the ancillary ligand was replaced with a different one, OR. However, in the

Table 1 Synthetic procedures and obtained metallosupramolecular isomer and polymorphic forms

[VO(SIH)(OR)]ₓ	OR	x	Procedure
1t·4CH₃OH	OCH₃	4	I
1β·0.25CH₃OH	OCH₃	n	II
2α	OC₂H₅	n	I or III
2β·0.25C₂H₅OH	OC₂H₅	n	II
3α	OC₃H₇	n	I or III
4α	OC₄H₉	n	I or II or III
4β	OC₄H₉	n	I
5β	OC₅H₁₁	n	I or III

Scheme 1 Structure of the H₂SIH ligand and synthetic pathways to oxovanadium(v) supramolecular species.

case of ethanol and butanol, it resulted in a mixture of polymorphs **2α** and **2β**·0.25CH$_3$OH, **4α** and **4β**, respectively. A similar result was obtained by higher alkoxo ligand substitution when submersing crystals in methanol. Polymer and tetramer with coordinated methoxo ligand were achieved as a mixture.

We were therefore interested in studying the thermally assisted structural transformation of [VO(SIH)(OCH$_3$)]$_4$·4CH$_3$OH (**1t**·4CH$_3$OH) in solvent-free conditions. Consistent with findings on its thermal stability (*vide infra*), a crystalline sample of **1t**·4CH$_3$OH was gradually heated from the ambient temperature up to 165 °C with a heating rate of 10 °C min^{-1}. After being held at that temperature for one hour, the amorphous residue of the thermally activated complex [VO(SIH)]$_x$ was immersed in the corresponding ROH for one week (Procedure III). This procedure resulted in the formation of **1t**, **2α**, **3α**, **4α**, and **5β** which were identified by IR-ATR and X-ray powder diffraction method (Fig. S4, see ESI†). The formation of polymers can be explained by the cleavage of the V–N$_{isonicotinoyl}$ bonds in the metallocycle and formation of new V–N$_{isonicotinoyl}$ bonds in solution. It is worth noting that the formation of a supramolecular architecture indirectly through the solid-state transformation of vanadium supramolecular complex has never been reported.

In the reaction between the NH$_4$VO$_3$ and hydrazone ligand in methanol, followed by the evaporation in an airstream, the [VO$_2$(HSIH)] (**6**) compound crystallized. A single-crystal X-ray study of **6** confirmed the structure to be mononuclear. However, it was previously reported (CSD refcode LAMLES).[59]

Description of molecular and crystal structures

High-quality single crystals suitable for single crystal X-ray diffraction were obtained for total of 7 compounds, namely **1t**·4CH$_3$OH, **2α**, **3α**, **4α**, **1β**·0.25CH$_3$OH, **2β**·0.25C$_2$H$_5$OH and **5β**. General and crystallographic data can be found in ESI, Tables S1–S2 and Fig. S5–S7.† Determined crystal structures represent a diverse set of metallosupramolecular assemblies based on the same building block – {VO(OR)(L)} (Fig. 2, top left). The geometry of the monomeric building unit is practically identical across the observed structures: vanadium center is situated in an expected *ONO* coordination environment provided by a doubly deprotonated hydrazonato ligand in its enolato-imino tautomeric form (Fig. S5†). In each compound, oligomerization or polymerization is facilitated through coordination of the nitrogen atom from an ancillary pyridyl functional group on the sixth coordination site of the oxovanadium(v) centre.

Tetranuclear complex **1t** crystallizes in the tetragonal space group *I*4̄. Although the complex has a fourth order rotoinversion symmetry (Fig. 2, top right), the complex conforms to a shape of a diagonally folded square, with vanadium centers significantly shifted from the tetramer equatorial plane (Fig. S7†). Moreover, the complex molecules are stacked along the ring axis, forming large channels comprising up to 20.7% of unit cell volume. This arrangement of molecules is certainly unexpected and could represent a new moment in supramolecular metal–organic frameworks (sMOF), and the detailed investigations are
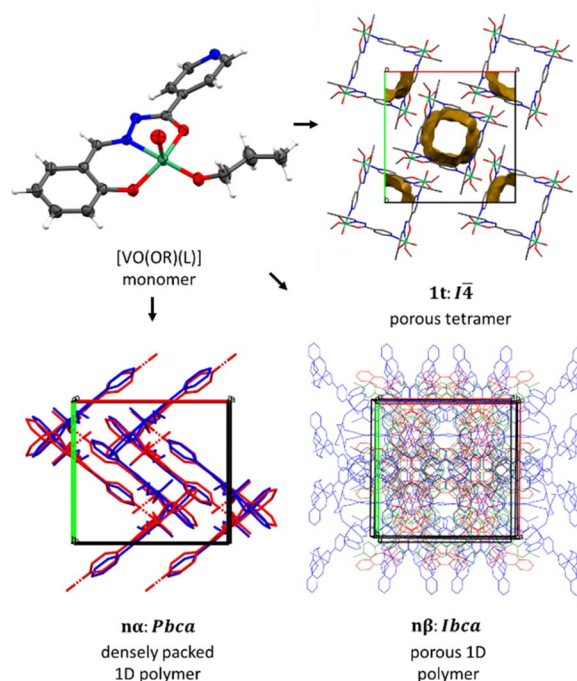

Fig. 2 [VO(OR)(L)] monomer (L = SIH) can oligomerize into porous tetramer **1t**, or polymerize into polymorphs **α** (densely packed 1D chains) or **β** (porous assembly of 1D chains). Structures of **α** and **β** are shown as structural overlays of complexes with 2 and 3 different alkoxy chain lengths, respectively, emphasizing the isostructurality of the assemblies.

underway. The contents of the void volume could not be modelled from the difference Fourier map, but according to the TGA analysis the voids are natively filled with residual solvent molecules with ratio V : CH$_3$OH equal to unity.

Besides this tetranuclear complex, two major groups of compounds representing (pseudo)polymorphic pairs were identified, **nα** and **nβ**, although a complete structural determination of both polymorphs was only achieved for compound **2**, namely **2α** and **2β**·0.25C$_2$H$_5$OH.

Crystallographic analysis showed that compounds in the **α** form crystallize as densely packed 1D polymeric chains in space group *Pbca*, whereas those in the **β** form crystallize in space group *Ibca* with a different arrangement of 1D polymeric chains, but with the same 2C1 underlying topology (Fig. 2, bottom, Fig. S6†). As evidenced by the structural data, as well as PXRD data, the isolated **α** and **β** solid forms are isostructural within each group, up to a difference in the alkoxy chain. The coordination environment of vanadium ion remains consistent throughout the structures. The arrangement of chains in **β** polymorphs allows for significant void volume in the structures. For instance, **1β** contains approximately 9.7% void volume, **2β** contains about 12.7%, and **5β** also has an appreciable void volume, but its determination is obstructed by disordered pentoxy chains, which partially occupy the voids. It is nevertheless inferred that **β**-type polymorphs generally permit the formation of channels enclosed by partially disordered alkoxy groups. As in the case of **1t**, the difference Fourier

map in the channels is featureless, so the final composition is inferred from the void volume, solvent molar volume and TGA analysis.

All three types of assemblies are characterized by the lack of strong or directed supramolecular interactions, as there are no suitable hydrogen bond donors. In line with the introductory findings, the lack of supramolecular interactions favours the existence of polymorphs. However, to the best of our knowledge, the α–β polymorphic system could be the first one where such a stark difference in porosity is observed. This fact, along with no significant stability differences between the polymorphs, could serve as motivation for investigation of this polymorphic system (and related systems lacking strong supramolecular interactions) as solid-state porosity-on-demand materials.

Principal component analysis

We focused on gaining a more profound comprehension of this reaction system. The reaction between NH_4VO_3 and H_2SIH (with initial reactant concentrations of 4.0×10^{-5} mol dm^{-3}) was studied in methanol at ambient temperature using time-dependent UV-Vis spectroscopy (Fig. 3). The time-dependent spectra were analyzed by employing principal component analysis, a 2nd-order tensor decomposition tool. The results

indicated that two principal components could accurately represent the initial dataset (comprising 221 spectra). These components accounted for more than 98% of the total variance in the original data.

The first principal component accounted for 80.79% of the total variance highlighting a significant reaction involving the coordination of the hydrazonato ligand to vanadium. The second component accounted for 17.35% of the total variance, reflecting a secondary reaction occurring within the system (Fig. 4). Furthermore, the analysis of the UV spectra from the V-hydrazonato complex showed a complete conversion of the initially formed hydrazonato complex into the related dioxovanadium(v) species in very dilute methanolic solutions.

Spectroscopic characterization

UV-Vis spectra. The UV-Vis spectra of H_2SIH and coordination complexes **1t** and **1–6** were recorded in methanol and acetonitrile. The results of these spectral analyses are illustrated in Fig. S8 and S9, see ESI.† The summarized spectral data, including maximum wavelengths (λ_{max}) and molar absorptivity values (ε), are presented in Table S4, see ESI.†

In methanolic solution, H_2SIH exhibits distinct absorption maxima at wavelengths of 214 nm, 288 nm, and 333 nm, along with several shoulder peaks (see ESI†). The absorption band at 214 nm is associated with $\pi \rightarrow \pi^*$ transitions occurring in the aromatic rings. The bands observed at 288 nm and 333 nm correspond to $\pi \rightarrow \pi^*$ and $n \rightarrow \pi^*$ transitions, respectively, which are associated with the azomethine and carbonyl functionalities.[60,61] In the spectra of methanolic solutions of complexes **1t** and **1–6**, these intraligand transitions are exhibited at around 230 nm and 320 nm alongside the band at about 404 nm that is assignable to charge transfer from the coordinated hydrazonato ligand to vanadium (LMCT band).[60]

NMR spectra. The ^1H NMR spectra of compounds **1t** and **1–5** in CD_3OD displayed a single set of well-resolved and upfield/downfield-shifted chemical resonances for the protons of coordinated SIH^{2-} unit. The azomethine H1 proton of the hydrazone-based ligand (SIH^{2-}) was significantly shifted downfield by 0.28 ppm. The protons H7,9 and H6,10 of the isonicotinoyl moiety were slightly upfield and downfield shifted, respectively, in comparison to the free ligand (Scheme S1,
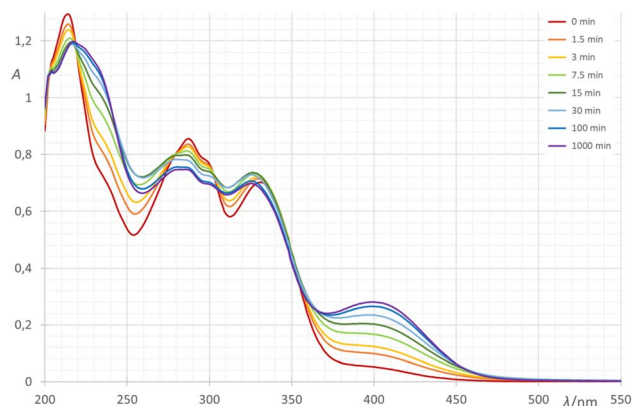

Fig. 3 Time-dependent UV-Vis spectra of a reaction mixture of NH_4VO_3 and H_2SIH in methanol at room temperature.
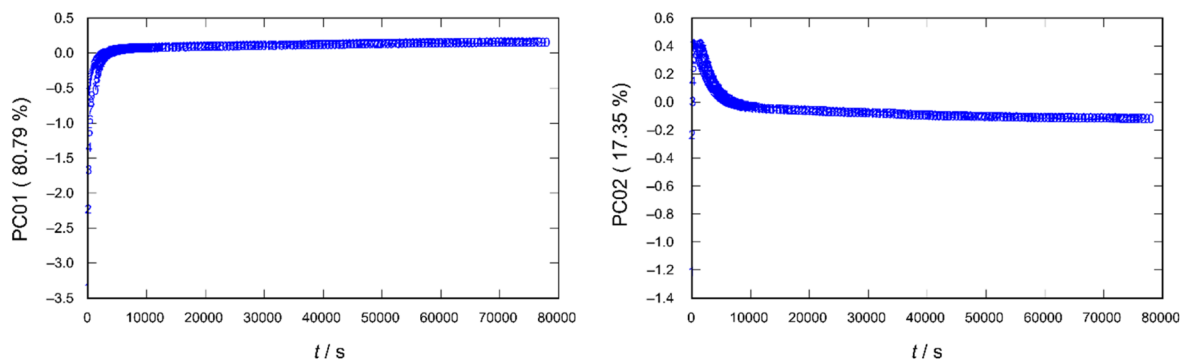

Fig. 4 Principal component scores for the reaction of NH_4VO_3 and H_2SIH in methanol at room temperature monitored in time by UV-Vis spectrophotometry.

Fig. S10, Table S4, in the ESI†). This indicates that in diluted CD$_3$OD solution the nitrogen atom is not coordinated to the metal ion. The phenyl protons H16 and H13 appeared as a doublet of doublets, while a triplet of doublets with a noticeable upfield shift was observed for H14 and H15.

The ^{1}H NMR spectra of **1–5** are similar, except for resonances attributed to free ROH. The ^{13}C NMR spectra revealed deshielding of the chemical shifts for C1, C4, and C12 carbons, with maximum shifts of 3.00 ppm, 6.81 ppm, and 5.99 ppm, respectively, because of metal complexation. On the other hand, in highly diluted deuterated methanol solutions, it appears that the coordination of the pyridine ring to the coordinatively unsaturated vanadium center is not maintained. The isonicotinoyl carbons C5–C10 exhibited minimal changes in chemical shifts compared to the free ligand, with a maximum of $\Delta\delta = 0.98$ ppm.

ATR-IR spectra. The O–H, =N–NH, and C=O bands (at 3200 cm^{-1}, 3180 cm^{-1}, and 1683 cm^{-1}, respectively),[58] which are characteristic of free hydrazone ligand H$_2$SIH, disappeared upon vanadium–ligand complexation (Fig. S11 and S12 in the ESI†). The presence of bands belonging to C=N$_{imine}$ (at about 1620 cm^{-1}), C–O$_{hydrazonato}$ (at about 1345 cm^{-1}), and C–O$_{phenolic}$ (at about 1275 cm^{-1}) in the spectra of **1t** and **1–5** indicated SIH^{2-} coordination to the metal centre *via* oxygen and nitrogen donor atoms.[21–23] This is further confirmed by the weaker intensity bands for V–N$_{imine}$ at 750 cm^{-1}, V–O$_{hydrazonato}$ at 580 cm^{-1}, and V–O$_{phenolato}$ at 560 cm^{-1}. The spectra also exhibited a medium-intensity stretching band at 1600 cm^{-1} associated with C=N of the isonicotinoyl pyridine ring moiety. This band is shifted to a lower wavenumber, when compared to free hydrazone, indicating coordination of the isonicotinic-nitrogen atom to the {VO}$^{3+}$ core. A medium intensity band observed at 970 cm^{-1} was assigned to N–N stretching vibrations.[62]

Bands at about 710 cm^{-1} characteristic for V–N bonds corroborated the metallosupramolecular complex formation. The coordination of RO$^-$ in complexes **1t** and **1–5** was supported by a new absorption band typical of C–O$_{OR}$ at approximately 1040 cm^{-1}.[63] This band was missing in the spectra of the thermally activated complex [VO(SIH)]$_x$. It should be noted that C–O$_{OR}$ stretching frequencies in metallosupramolecular species slightly differ from those in the corresponding free alcohol.

The spectra of complexes **1t** and **1–5** displayed intense bands in the region of 970–956 cm^{-1} (Fig. S11 and S12†), which were characteristic of the {VO}$^{3+}$ core.[64] It should be noted that there is a certain similarity of spectra belonging to the same series of polymorphs.

It is worth noting that the absence of coordinated isonicotinoyl moiety and alkoxide co-ligand in the case of the mononuclear complex **6** resulted in a slightly lower intensity stretching bands at 953 cm^{-1} and 942 cm^{-1} belonging to the {O=V=O}$^+$ core. The bands characteristic for C–O$_{phenolic}$, C=N, and C–O$_{hydrazone}$ were accompanied by the broad band in the range of 2400–2600 cm^{-1} assigned to the N–H stretching vibration of the protonated HSIH$^-$ ligand.[65]

Thermogravimetric analyses. Metallocycle **1t**·4CH$_3$OH and polymers **1β**·0.25CH$_3$OH and **2β**·0.25C$_2$H$_5$OH, when left in

a desiccator at room temperature for a weak, showed the gradual loss of solvent of crystallization. Whereas crystals of **1β**·0.25CH$_3$OH and **2β**·0.25C$_2$H$_5$OH were stable at −15 °C, in the case of metallocycle **1t**·4CH$_3$OH partial desolvation of crystals occurred and yielded **1t**·2CH$_3$OH.

The thermal stabilities of all compounds were studied using thermogravimetric analysis (Fig. S13–S17 in the ESI†) by heating the crystalline sample in the temperature range of 25–600 °C under an oxygen atmosphere. The TGA analysis of solvates showed a steady decline at the beginning of the thermogram due to the loss of the lattice solvent molecules followed by the escape of oxidized alkoxide products in the temperature ranges of 29–153 °C and 154–237 °C (for **1t**·2CH$_3$OH), 25–77 °C and 148–256 °C (for **1β**·0.25CH$_3$OH), and 40–144 °C and 148–259 °C (for **2β**·0.25C$_2$H$_5$OH). The onset temperatures of the first step in TGA are very low, signifying the presence of weak noncovalent interactions in the solid state.

All desolvated polymeric compounds exhibited a comparable pattern of thermal decomposition steps. The mass loss process, due to the oxidation of one alkoxide for each metal–organic unit, started above 100 °C (at 148 °C (for **1β**), 165 °C (for **2α**), 148 °C (for **2β**), 185 °C (for **3α**), 135 °C (for **4α**), 114 °C (for **4β**), 149 °C (for **5β**)) with the butoxide derivative being the most unstable and propoxide the most stable. This step was followed by the final hydrazone decomposition of the corresponding complex.

Catalytic studies. To examine the catalytic behaviour of synthesized vanadium complexes, the study utilized complexes **1t** and **1β**, whose activity was compared to the compounds [VO$_2$(HSIH)] (**6**), [MoO$_2$(SIH)]$_n$, [VO(SIH)]$_x$ and V$_2$O$_5$. The objective was to evaluate the catalytic efficiency of these complexes in benzyl-, 2-nitrobenzyl-, 2-chlorobenzyl and 2-methylbenzyl alcohol oxidations. Benzyl alcohol was selected as the reference substrate due to its relatively simple structure and neutral electronic properties, providing a baseline for comparison. The inclusion of 2-nitrobenzyl and 2-chlorobenzyl alcohols was intended to explore the influence of electron-withdrawing substituents on the reactivity and behaviour of the system, with the nitro and chloro-groups serving as prototypical electron-withdrawing moieties. Conversely, 2-methylbenzyl alcohol was chosen to evaluate the effect of an electron-donating substituent, as the methyl group can impart steric and inductive effects that modulate electronic density in the aromatic ring. This systematic selection enabled a comprehensive investigation of electronic substituent effects on the substrate's chemical properties and reaction mechanisms.

Benzyl alcohol oxidation. The oxidation of benzyl alcohol was systematically studied using various oxidizing agents, including *tert*-butyl hydroperoxide (TBHP) in both aqueous and decane solutions, as well as hydrogen peroxide (H$_2$O$_2$). When TBHP in water was employed as the oxidant, the influence of different solvents, such as toluene, acetonitrile, and methanol, was explored to assess their impact on the reaction. For the oxidation involving hydrogen peroxide, acetonitrile was added to the reaction mixture as a co-solvent. These variations were investigated to evaluate how the choice of oxidant and solvent environment affects the efficiency and selectivity of the
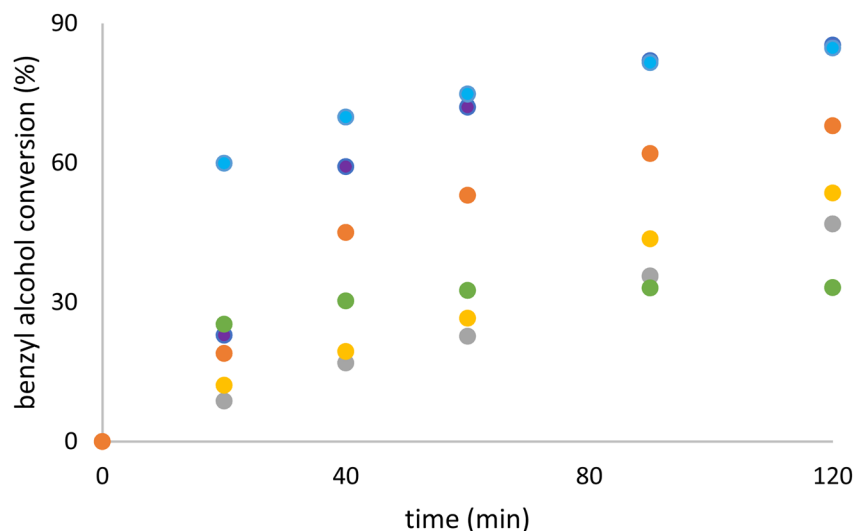
Fig. 5 Kinetic profile of benzyl alcohol conversion with catalyst **1t**. Light blue presents the reaction with TBHP in decane, purple with TBHP in water, orange with TBHP in water and toluene, yellow with TBHP in water and methanol, grey with TBHP in water and acetonitrile and green with hydrogen peroxide and acetonitrile.

oxidation process. The obtained results are compiled in Fig. 5 and Table 2.

Catalysts **1t** and **1β** show consistently high conversions across various conditions, particularly with TBHP in decane (85%) and TBHP in water (>85%). These values are comparable to **6** [VO$_2$(HSIH)], suggesting its effectiveness. TOF$_{20 \text{ min}}$ values are among the highest (346 for **1t** and 402 for **1β** with TBHP in decane), indicating rapid catalytic activity. Selectivity remains moderate to low across most conditions. For instance, aldehyde selectivity for **1t** is only 16% with TBHP in decane and 18% with TBHP in water. This indicates the catalyst prioritizes reactivity over specificity. Catalyst **1β** performs slightly better than **1t**, with TBHP in decane, it achieves a conversion of 60% and a selectivity of 38%, striking a better balance between reactivity and selectivity. TOF$_{20 \text{ min}}$ values for **1β** (402 with TBHP in decane) are larger than **1t**, making it a faster-acting catalyst in benzyl alcohol oxidation. The selectivity parameter is similar for **1β** than **1t** in aqueous TBHP-driven systems. Fig. 5 illustrates the performance comparison of the tested conditions for catalyst **1t**. The data reveal that **1t** exhibits the highest activity when TBHP is utilized in decane or water as the oxidant, whereas its activity is significantly reduced when H$_2$O$_2$ and MeCN are employed. Furthermore, the choice of solvent added to TBHP in water substantially affects the conversion rate, with the activity following the order: toluene > methanol > acetonitrile. However, aldehyde selectivity is the highest when TBHP in water and MeCN or MeOH were applied as oxidants. Catalyst [VO$_2$(HSIH)] (**6**) showed good conversion rates in oxidant-rich conditions, especially with TBHP in water and decane, 75 and 84%, respectively. Aldehyde selectivity in the same oxidants is moderate (13 and 29%, respectively), highlighting its preference for reactivity over product-desired aldehyde.

[MoO$_2$(SIH)]$_n$ has low conversion parameters under all the tested conditions, although the aldehyde selectivity is quite high, spanning to 90% when hydrogen peroxide with the

addition of acetonitrile is used as an oxidant. It can be noted that the Mo catalyst is not very active for the benzyl alcohol oxidations, no matter the oxidant chosen or solvent added to the reaction mixture.

V$_2$O$_5$ exhibits high conversion rates with TBHP in water (78%) and decane (82%). Conversion decreases in aqueous TBHP-driven systems when the solvent is added. Aldehyde selectivity with TBHP in water is 27%, while in decane is 20%. In contrast, the addition of solvent to TBHP in water increases the selectivity (79% in toluene, 65% in MeCN, 55% in MeOH). It has to be noted that the aldehyde selectivity remains the same through all the reactions and does not decrease with time, highlighting that the overoxidation of aldehyde to the corresponding carboxylic acid is not present.

[VO(SIH)]$_x$ has been tested with TBHP in water, decane and H$_2$O$_2$. It can be observed that in TBHP benzyl alcohol oxidation is quite high, but the aldehyde selectivity remains low, while with H$_2$O$_2$ as an oxidant, the conversion of benzyl alcohol and aldehyde selectivity achieve similar values (30% of selectivity and 42% of conversion).

2-Nitrobenzyl, 2-chlorobenzyl and 2-methylbenzyl alcohol oxidations. Two different oxidants, TBHP in water and TBHP in decane were evaluated, Fig. 6 and Table 3. The reactions were monitored for 2 hours, as for some tested catalysts, no aldehyde remained in the reaction mixture beyond this time due to its oxidation to carboxylic acid, Table 3.

For 2-chlorobenzyl alcohol, the catalysts **1t**, **1β**, [VO$_2$(HSIH)], and [VO(SIH)]$_x$ achieved high conversion rates (>84%) with both oxidants. Selectivity toward aldehyde at the reaction's conclusion was moderate regardless of the oxidant. However, after 20 minutes, aldehyde selectivity was notably higher with TBHP in water, peaking at 96% with [VO$_2$(HSIH)]. V$_2$O$_5$ exhibited a higher conversion rate with TBHP in decane compared to water (86% vs. 58%), while aldehyde selectivity was superior with TBHP in water (62%) compared to decane (29%). TON

Table 2   Catalytic results of benzyl alcohol oxidation. Reaction conditions: time, 2 h; temperature, 80 °C, n(catalyst)/n(benzyl alcohol)/n(oxidant) = 0.1 mmol/20 mmol/40 mmol

Catalyst	1t		1β		6		$[MoO_2(SIH)]_n$		V_2O_5		$[VO(SIH)]_x$	
Time/min	120	20	120	20	120	20	120	20	120	20	120	20
TBHP in water												
No solvent												
Conversion[a]	85	23	90	70	75	16	14	9	78	3	79	36
Selectivity[b]	18	74	12	33	29	77	50	31	27	2	26	60
TOF$_{20\ min}$[c]	140		391		92		59		42		223	
TON[d]	174		168		149		30		323		163	—
Toluene												
Conversion	68	19	63	16	50	3	5	1	30	7		
Selectivity	3	70	43	70	56	89	47	63	79	72		
TOF$_{20\ min}$	114		93		21		3		35			
TON	136		123		100		10		52			
MeCN												
Conversion	47	9	54	11	39	12	6	3	43	8		
Selectivity	66	90	58	85	61	35	53	39	65	63		
TOF$_{20\ min}$	46		61		70		17		49			
TON	83		102		75		12		82			
MeOH												
Conversion	53	12	52	4	47	3	10	2	45	8		
Selectivity	49	68	49	90	54	88	30	48	55	63		
TOF$_{20\ min}$	63		24		17		15		45			
TON	93		102		91		21		82			
TBHP in decane												
No solvent												
Conversion	85	60	87	67	84	40	14	6	82	46	82	49
Selectivity	16	38	13	31	16	48	68	46	20	53	19	39
TOF$_{20\ min}$	346		402		226		34		282		284	
TON	163		175		161		26		169		160	
H_2O_2												
MeCN												
Conversion	33	25	38	30	77	28	11	4	33	28	42	11
Selectivity	40	42	36	38	26	49	90	99	39	48	30	76
TOF$_{20\ min}$	165		197		181		23		172		67	
TON	72		81		168		22		68		85	

[a] Substrate consumed at the end of the reaction. [b] Formed aldehyde per converted alcohol at the end of the reaction. [c] n(substrate) transformed/n(catalyst)/time(h) at 20 min. [d] n(substrate) transformed/n(catalyst) at the end of reaction.
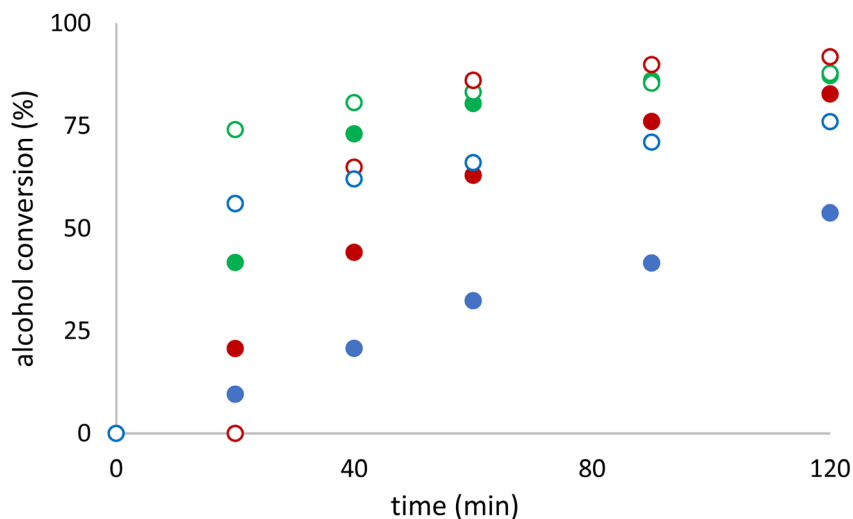
Fig. 6 Kinetic profile of benzyl alcohol conversion with catalyst **1t**. Blue circles presents the reaction with 2-nitrobenzyl alcohol, green circles with 2-chlorobenzyl alcohol and red circles with 2-methylbenzyl alcohol. Full circles are reaction with TBHP in water and empty circles with TBHP in decane.

values for the catalysts **1t**, **1β**, $[VO_2(HSIH)]$, and $[VO(SIH)]_x$ are similar, no matter the oxidant used, achieving values 171-213, while V_2O_5 shows the lowest value of 126 with TBHP in water. TOF values for all the catalysts with TBHP in decane are almost two times higher than with TBHP in water.

For 2-nitrobenzyl alcohol, the catalytic activity in water is notably lower compared to decane, whereas selectivity toward the aldehyde shows the opposite trend. The oxidative conversion of aldehyde to carboxylic acid, evident from the comparison of selectivity parameters at 20 and 120 minutes, is less pronounced than in the case of 2-chlorobenzyl alcohol. This difference is likely due to the electron-withdrawing nitro group stabilizing the aldehyde, thereby reducing its susceptibility to overoxidation. Catalysts **1t**, $[VO_2(HSIH)]$, and $[VO(SIH)]_x$ demonstrate similar performance trends. Alcohol conversions in water hover around 50%, with aldehyde selectivity at the reaction's conclusion reaching approximately 65%. In decane, alcohol conversions increase to ~58%, while aldehyde selectivity decreases significantly to ~30%. Catalyst **1β** displays consistent activity irrespective of the oxidant, achieving alcohol conversions exceeding 70%. However, aldehyde selectivity is higher in water, reaching 42% at the reaction's end. Notably, at 20 minutes, aldehyde selectivity in water is nearly maximal, peaking at 98%. The TON values for all catalysts are lower for 2-nitrobenzyl alcohol than for 2-chlorobenzyl alcohol, with slightly higher values observed in decane. The $TOF_{20\ min}$ values, however, are significantly higher with TBHP in decane, reaching a maximum of 298 for **1t**. These findings highlight the delicate interplay between catalyst, oxidant, and substrate electronic properties in determining reaction efficiency and selectivity.

A comparison of the oxidation reactions of 2-chlorobenzyl alcohol and 2-nitrobenzyl alcohol reveals that 2-nitrobenzyl alcohol is a superior substrate for selective oxidation to aldehydes. This superiority arises from the strong electron-withdrawing properties of the nitro group, which significantly increase the electrophilicity of the benzyl carbon, thereby facilitating the oxidation process under milder conditions. Furthermore, the aldehyde product derived from 2-nitrobenzyl alcohol is stabilized by the resonance and inductive effects of the nitro group, reducing its susceptibility to overoxidation into the corresponding carboxylic acid. In contrast, the weaker electron-withdrawing inductive effect of the chloro substituent in 2-chlorobenzyl alcohol renders the benzyl carbon less electrophilic, necessitating severe oxidation conditions and resulting in a less stable aldehyde product.

The conversion of 2-methylbenzyl alcohol is high, whether TBHP is used in water or decane. However, the aldehyde selectivity showed very low values. The obtained results seem to not favour 2-methylbenzyl alcohol as a substrate. The methyl group is an electron-donating group due to its inductive effect that could reduce electrophilicity at the benzyl position and destabilization of the intermediates compared to the 2-chloro- and 2-nitro-benzyl alcohol. Furthermore, the methyl group introduces significant steric hindrance near the benzyl alcohol group. As expected, the desired aldehyde is less stabilized and more prone to overoxidation to the carboxylic acid under strong oxidative conditions present in the reaction.

Experimental

General details

$[VO(acac)_2]$, $[MoO_2(SIH)]_n$, and salicylaldehyde isonicotinoyl hydrazone (H_2SIH), were synthesized according to the procedures described in the literature.[57,58,66] Ammonium metavanadate, salicylaldehyde, and isonicotinoyl hydrazide were commercially available. All chemicals and solvents were used without further purification. They were purchased from Alfa Aesar or Aldrich. Details about the instruments and characterization methods (elemental and thermal analyses, ATR-IR, UV, NMR spectroscopies, PXRD, and SCXRD methods) and obtained data can be found in the ESI.† The crystals obtained from the

Table 3 Catalytic results of 2-chloro, 2-nitro and 2-methyl benzyl alcohol oxidation. Reaction conditions: time, 2 h; temperature, 80 °C, n(catalyst)/n(alcohol)/n(oxidant) = 0.0165 mmol/3.30 mmol/6.60 mmol

Catalyst	1t		1β		6		V_2O_5		[VO(SIH)]$_x$	
Time/min	120	20	120	20	120	20	120	20	120	20
2-Chloro benzyl alcohol										
TBHP in water										
Conversion[a]	87	42	89	55	84	44	58	7	90	45
Selectivity[b]	32	73	26	58	37	96	62	96	27	73
TOF$_{20\ min}$[c]	251		395		28		44		275	
TON[d]	176		213		173		126		181	
TBHP in decane										
Conversion	88	74	87	61	88	51	86	68	89	74
Selectivity	30	42	31	40	26	58	29	39	24	43
TOF$_{20\ min}$	460		382		334		439		422	
TON	182		180		192		184		171	
2-Nitro benzyl alcohol										
TBHP in water										
Conversion	54	10	71	24	48	11	22	3	53	17
Selectivity	65	98	41	87	70	70	93	51	64	60
TOF$_{20\ min}$	55		132		66		19		93	
TON	103		130		93		39		96	
TBHP in decane										
Conversion	76	56	78	50	78	24	71	39	79	51
Selectivity	32	48	28	42	29	57	36	69	28	49
TOF$_{20\ min}$	298		240		142		201		273	
TON	133		125		157		122		142	
2-Methyl benzyl alcohol										
TBHP in water										
Conversion	83	21	93	30	90	6	78	3	93	32
Selectivity	8	73	3	60	5	97	12	87	33	53
TOF$_{20\ min}$	117		170		27		15		185	
TON	156		178		144		144		184	
TBHP in decane										
Conversion	93	65	95	41	86	67	93	67	93	72
Selectivity	3	7	2	22	6	11	3	15	7	8
TOF$_{20\ min}$	429		258		479		441		463	
TON	205		200		207		205		199	

[a] Substrate consumed at the end of the reaction. [b] Formed aldehyde per converted alcohol at the end of the reaction. [c] n(substrate) transformed/n(catalyst)/time(h) at 20 min. [d] n(substrate) transformed/n(catalyst) at the end of reaction.

reaction were used directly for the IR-ATR and X-ray crystallographic studies. The samples for elemental analysis were completely desolvated until constant weight and were analysed. The samples for TG measurements were transferred into a desiccator and placed in a freezer (at −15 °C).

Synthesis of the metallosupramolecular compounds

Procedure I. NH_4VO_3 (0.023 g, 0.20 mmol) was added to a solution of H_2SIH (0.051 g, 0.21 mmol) in alcohol (30 mL). The reaction mixture was refluxed for 3 h and left to stand at room temperature. The solution was concentrated under reduced pressure (see below for details). Dark red-black crystals, formed over one week, were isolated *via* filtration and dried to constant mass in a desiccator (at −15 °C). This procedure afforded **1t**·4CH$_3$OH, **2α**, **3α**, **4α**, **4β**, and **5β**.

Procedure II. [VO(acac)$_2$] (0.053 g, 0.20 mmol) and H_2SIH (0.0483 g, 0.20 mmol) were suspended in alcohol (3 mL). The reaction mixture was stirred with a glass rod in a in a nitrogen-filled glovebox for 15 minutes and the suspension was left to stand at room temperature in a closed flask. Dark red-black crystals formed over several weeks were isolated *via* filtration and dried to constant mass in a desiccator (at −15 °C). This procedure afforded **1β**·0.25CH$_3$OH and **2β**·0.25C$_2$H$_5$OH.

Procedure III. The crystalline sample of [VO(SIH)(OCH$_3$)]$_4$·4CH$_3$OH (0.02 g, 0.014 mmol) was heated for one hour at 165 °C and the obtained solid was cooled and then added to 1 mL of the corresponding primary alcohol ROH (C$_n$H$_{2n+1}$OH, n = 1–5). The sample of each setup was taken out after one week and immediately examined by ATR-IR spectroscopy and PXRD method. This afforded the corresponding compounds **1t**, **2α**, **3α**, **4α**, and **5β**, respectively.

[VO(SIH)(OCH$_3$)]$_4$·4CH$_3$OH (1t·4CH$_3$OH). The complex was prepared by *Procedure I* in methanol. The solution was concentrated after two days to about 5 mL. Yield: 0.040 g; 54%.

Anal. calcd for **1t**, $C_{56}H_{48}N_{12}O_{16}V_4$ (1348.817): C, 49.87; H, 3.59; N, 12.46. Found: C, 49.68; H, 3.27; N, 12.33%. TG for **1t**·2CH$_3$OH: CH$_3$OH, 4.18 (calcd 4.54%), CH$_3$O, 8.53 (calcd 8.79%); V_2O_5, 25.88% (calcd 25.75%). Selected IR data (cm^{-1}): 1622, 1601 (C=N), 1349 (C–O$_{hydrazone}$), 1274 (C–O$_{phenolate}$), 1041 (C–O$_{alkoxo}$), 964 (N–N), 956 (V=O), 759 (V–N$_{imine}$), 713 (V–N$_{isonicotinoyl}$), 627 (V–O)$_{alkoxo}$, 582 (V–O)$_{hydrazonato}$, 563 (V–O)$_{phenolato}$.

[VO(SIH)(OCH$_3$)]$_n$·0.25CH$_3$OH (1β·0.25CH$_3$OH). The complex was prepared by *Procedure II* in methanol. Yield: 0.056 g; 81%. Anal. calcd for **1β**, $C_{14}H_{12}N_3O_4V$ (337.204): C, 49.87; H, 3.59; N, 12.46. Found: C, 49.68; H, 3.25; N, 12.12%. TG for **1β**·0.25CH$_3$OH: CH$_3$OH, 1.97 (calcd 2.32%), CH$_3$O, 8.58 (calcd 8.99%); V_2O_5, 25.99% (calcd 26.34%). Selected IR data (cm^{-1}): 1616, 1600 (C=N), 1345 (C–O$_{hydrazone}$), 1279 (C–O$_{phenolate}$), 1051 (C–O$_{alkoxo}$), 973 (N–N), 959 (V=O), 750 (V–N$_{imine}$), 709 (V–N$_{isonicotinoyl}$), 623 (V–O)$_{alkoxo}$, 570 (V–O)$_{hydrazonato}$, 559 (V–O)$_{phenolato}$.

[VO(SIH)(OC$_2$H$_5$)]$_n$ (2α). The complex was prepared by *Procedure I* in ethanol. The solution was concentrated after one day to about 20 mL and a small amount of precipitated solid filtered the next day. The product **2α** was obtained from the filtrate. Yield: 0.027 g; 39%. Anal. calcd for **2α**, $C_{15}H_{14}N_3O_4V$ (351.230): C, 51.29; H, 4.02; N, 11.96. Found: C, 51.03; H, 3.86; N, 11.78%. TG for **2α**: C$_2$H$_5$O, 12.56 (calcd 12.83%); V_2O_5, 25.99% (calcd 25.89%). Selected IR data (cm^{-1}): 1620, 1599 (C=N), 1349 (C–O$_{hydrazone}$), 1278 (C–O$_{phenolate}$), 1046 (C–O$_{alkoxo}$), 969 (N–N, V=O), 756 (V–N$_{imine}$), 710 (V–N$_{isonicotinoyl}$), 633 (V–O)$_{alkoxo}$, 587 (V–O)$_{hydrazonato}$, 562 (V–O)$_{phenolato}$.

[VO(SIH)(OC$_2$H$_5$)]$_n$·0.25C$_2$H$_5$OH (2β·0.25C$_2$H$_5$OH). The complex was prepared by *Procedure II* in ethanol. Yield: 0.063 g; 87%.

Anal. calcd for **2β**, $C_{15}H_{14}N_3O_4V$ (351.230): C, 51.29; H, 4.02; N, 11.96. Found: C, 50.98; H, 3.79; N, 11.75%. TG for **2β**·0.25C$_2$H$_5$OH: C$_2$H$_5$OH, 3.12 (calcd 3.18%), C$_2$H$_5$O, 12.56 (calcd 12.42%); V_2O_5, 24.82% (calcd 25.07%). Selected IR data (cm^{-1}): 1615, 1598 (C=N), 1344 (C–O$_{hydrazone}$), 1277 (C–O$_{phenolate}$), 1038 (C–O$_{alkoxo}$), 974 (N–N), 964 (V=O), 750 (V–N$_{imine}$), 709 (V–N$_{isonicotinoyl}$), 630 (V–O)$_{alkoxo}$, 574 (V–O)$_{hydrazonato}$, 560 (V–O)$_{phenolato}$.

[VO(SIH)(OC$_3$H$_7$)]$_n$ (3α). The complex was prepared by *Procedure I* in 1-propanol. The solution was concentrated after one day to about 20 mL. Yield: 0.062 g; 85%. Anal. calcd for **3α**, $C_{16}H_{16}N_3O_4V$ (365.257): C, 52.61; H, 4.42; N, 11.50. Found: C, 52.45; H, 4.32; N, 11.36%. TG for **3α**: C$_3$H$_7$O, 16.44 (calcd 16.18%); V_2O_5, 24.62% (calcd 24.90%). Selected IR data (cm^{-1}): 1617, 1596 (C=N), 1348 (C–O$_{hydrazone}$), 1277 (C–O$_{phenolate}$), 1049 (C–O$_{alkoxo}$), 9727 (N–N), 970 (V=O), 756 (V–N$_{imine}$), 706 (V–N$_{isonicotinoyl}$), 629 (V–O)$_{alkoxo}$, 590 (V–O)$_{hydrazonato}$, 562 (V–O)$_{phenolato}$.

[VO(SIH)(OC$_4$H$_9$)]$_n$ (4α). (a) The complex was prepared by *Procedure I* in 1-butanol. After the reaction, the solution was left at room temperature for 5 days and evaporated to 10 mL. The resulting crystalline product was filtered the next day. Yield: 0.054 g; 71%. (b) The complex was also prepared by *Procedure II* in 1-butanol. Yield: 0.053 g; 70%. Anal. calcd for **4α**, $C_{17}H_{18}N_3O_4V$ (379.284): C, 53.83; H, 4.78; N, 11.08. Found: C, 52.62; H, 4.56; N, 10.84%. TG for **4α**: C$_4$H$_9$O, 18.85 (Calcd. 19.28%); V_2O_5, 24.24% (Calcd. 23.98%). Selected IR data (cm^{-1}): 1614, 1598 (C=N), 1348 (C–O$_{hydrazone}$), 1277 (C–O$_{phenolate}$), 1042 (C–O$_{alkoxo}$), 972 (N–N), 969 (V=O), 754 (V–N$_{imine}$), 699 (V–N$_{isonicotinoyl}$), 630 (V–O)$_{alkoxo}$, 585 (V–O)$_{hydrazonato}$, 561 (V–O)$_{phenolato}$.

[VO(SIH)(OC$_4$H$_9$)]$_n$ (4β). The complex was prepared by *Procedure I* in 1-butanol. After completion of the reaction, the solution was evaporated to about 10 mL the same day. The resulting crystalline product was filtered the next day. Yield: 0.023 g; 30%. Anal. calcd for **4β**, $C_{17}H_{18}N_3O_4V$ (379.284): C, 53.83; H, 4.78; N, 11.08. Found: C, 53.66; H, 4.43; N, 10.88%.

TG for **4β**: C$_4$H$_9$O, 19.12 (calcd 19.28%); V_2O_5, 24.32% (calcd 23.98%). Selected IR data (cm^{-1}): 1621, 1598 (C=N), 1343 (C–O$_{hydrazone}$), 1276 (C–O$_{phenolate}$), 1060 (C–O$_{alkoxo}$), 968 (N–N), 957 (V=O), 750 (V–N$_{imine}$), 694 (V–N$_{isonicotinoyl}$), 629 (V–O)$_{alkoxo}$, 577 (V–O)$_{hydrazonato}$, 560 (V–O)$_{phenolato}$.

[VO(SIH)(OC$_5$H$_{11}$)]$_n$ (5β). The complex was prepared by *Procedure I* in 1-pentanol. The solution was concentrated after one day to about 10 mL. Yield: 0.053 g; 67%. Anal. calcd for **5β**, $C_{18}H_{20}N_3O_4V$ (393.310): C, 54.97; H, 5.13; N, 10.68. Found: C, 54.77; H, 4.96; N, 10.48%. TG for **5β**: C$_5$H$_{11}$O, 21.85 (calcd 22.16%); V_2O_5, 23.28% (calcd 23.12%). Selected IR data (cm^{-1}): 1621, 1598 (C=N), 1344 (C–O$_{hydrazone}$), 1275 (C–O$_{phenolate}$), 1040 (C–O$_{alkoxo}$), 968 (N–N), 958 (V=O), 749 (V–N$_{imine}$), 694 (V–N$_{isonicotinoyl}$), 629 (V–O)$_{alkoxo}$, 578 (V–O)$_{hydrazonato}$, 560 (V–O)$_{phenolato}$.

Synthesis of the mononuclear compound

[VO$_2$(HSIH)] (6). NH$_4$VO$_3$ (0.023 g, 0.2 mmol) was added to a solution of H$_2$SIH (0.057 g, 0.21 mmol) in methanol (30 mL) and the reaction mixture was left to stand at room temperature for two weeks. The obtained solution was concentrated in an airstream to a third of its volume. An orange powdered product formed at room temperature over one week. Complex **6** was isolated and dried to constant weight. Yield: 0.025 g; 38%. Anal. calcd for **6**, $C_{13}H_{10}N_3O_4V$ (323.177): C, 48.31; H, 3.12; N, 13.00. Found: C, 48.13; H, 3.02; N, 12.87%. TG for **6**: V_2O_5, 27.90% (calcd 28.13%). Selected IR data (cm^{-1}): 1635, 1603 (C=N), 1351 (C–O$_{hydrazone}$), 1258 (C–O$_{phenolate}$), 969 (N–N), 953, 942 (V=O), 739 (V–N$_{imine}$), 571 (V–O$_{hydrazonato}$), 555 (V–O$_{phenolato}$).

Catalytic investigation

Reaction protocols for different alcohols

Benzyl alcohol. A reaction mixture was prepared with benzyl alcohol (2.16 g, 20 mmol), biphenyl (0.1152 g, 0.75 mmol) as the internal standard, and catalyst (0.1 mmol). The mixture was heated to 80 °C prior to the addition of aqueous *tert*-butyl hydroperoxide (TBHP, 70% w/w, 5.54 mL, 40 mmol) or heated to 70 °C before the addition of hydrogen peroxide (H$_2$O$_2$) (4.12 mL, 40 mmol) in the presence of 3 mL of acetonitrile.

2-Nitrobenzyl alcohol. A reaction mixture was prepared with 2-nitrobenzyl alcohol (0.51 g, 3.3 mmol), acetophenone (0.412 g, 3.43 mmol) as the internal standard, and catalyst (0.0165 mmol). The mixture was heated to 80 °C before the addition of aqueous TBHP (70% w/w, 0.91 mL, 6.6 mmol).

2-Chlorobenzyl alcohol. A reaction mixture was prepared with 2-chlorobenzyl alcohol (0.47 g, 3.3 mmol), acetophenone (0.412 g, 3.43 mmol) as the internal standard, and catalyst (0.0165 mmol). The mixture was heated to 80 °C prior to the addition of aqueous TBHP (70% w/w, 0.91 mL, 6.6 mmol).

2-Methylbenzyl alcohol. A reaction mixture was prepared with 2-methylbenzyl alcohol (0.40 g, 3.3 mmol), dodecane (0.225 g, 1.34 mmol) as the internal standard, and catalyst (0.0165 mmol). The mixture was heated to 80 °C prior to the addition of aqueous TBHP (70% w/w, 0.91 mL, 6.6 mmol).

The reaction progress was monitored over a two-hour period by collecting 0.1 mL aliquots of the organic phase at predefined time intervals (0, 20, 40, 60, and 120 minutes). Each aliquot was diluted with 1.4 mL of diethyl ether and subjected to gas chromatography (GC) analysis to assess the conversion and formation of reaction products.

Principal component analysis

Data acquired through time-dependent UV-Vis spectrophotometry during the monitored chemical reaction were exported in ASCII format and arranged into a matrix of numerical entries. This process resulted in a 2nd-order data tensor characterized by dimensions corresponding to the number-of-spectra × number-of-wavelengths. We then applied principal component analysis (PCA), a second-order tensor reduction technique, to decompose the dataset. PCA facilitates the identification of the best linear projections for a high-dimensional data set based on the least-squares approach. The resulting scores represent the projections of the original sample points on the principal component (PC) direction, thereby enabling a comprehensive description of the reactions in a reduced space. Consequently, each point in the score plots corresponds to one sample UV-Vis spectra. Data were mean-centered and PCA of the covariance matrix was performed utilizing the NIPALS algorithm, which was implemented within our software application, *moonee*.[67]

Conclusions

This research contributes to a better understanding of the vanadium-based metallosupramolecular polymorphic assemblies, particularly regarding their formation and properties. Namely, two series of isostructural oxovanadium(v) coordination 1D zig–zag chain polymers were synthesized. These include $[VO(SIH)(OR)]_n$, with R representing different alkyl groups (R = CH_3 ($1\beta \cdot 0.25CH_3OH$), C_2H_5 (2α and $2\beta \cdot 0.25C_2H_5OH$), C_3H_7 (3α), C_4H_9 (4α and 4β), and C_5H_{11} (5β)). The synthesis involved combining salicylaldehyde isonicotinoylhydrazonate (SIH^{2-}) and the corresponding alkoxide (OR^-) with $\{VO\}^{3+}$ units. The similarity observed in the powder diffractograms across the series allowed the identification of each compound's polymorphic type. Although detailed studies are still needed, initial results suggest that the formation of the pure phase may be controlled by the suitable reaction conditions – solution concentrations, crystallization temperatures, evaporation rates, solvent selection, and the chosen synthesis method. The occurrence of concomitant polymorphs likely arises from the

capacity of the $\{VO\}^{3+}$ ion and SIH^{2-} ligand to form two crystalline phases with only slight differences in formation energy. Additionally, a phase-pure metallocyclic supramolecular isomer $[VO(SIH)(OCH_3)]_4 \cdot 4CH_3OH$ ($1t \cdot 4CH_3OH$), was identified. This compound features the interconnection of the mononuclear units into 0D squares through V–N$_{isonicotinoyl}$ coordination bonds, which adds to the diversity of the compounds studied. The research also emphasizes the potential of vanadium-based metallosupramolecular architectures in catalytic applications, further contributing to a better understanding of the structure–activity relationships in these complex systems.

Data availability

The data supporting this article have been included as part of the ESI.† Crystallographic data for $1t \cdot 4CH_3OH$, 2α, 3α, 4α, $1\beta \cdot 0.25CH_3OH$, $2\beta \cdot 0.25CH_3CH_2OH$ and 5β have been deposited at the Cambridge Structural Data base under with deposition numbers CCDC 2367532–2367538.

Author contributions

Edi Topić: investigation, writing – original draft preparation, review and editing. Josipa Sarjanović: investigation and formal analysis. Danijela Musija: investigation and formal analysis, and writing – original draft preparation. Mirna Mandarić: investigation and formal analysis. Tomica Hrenar: chemometric analysis, writing – original draft preparation, visualization. Jana Pisk: investigation, supervision, formal analysis, writing – original draft preparation. Višnja Vrdoljak: conceptualization, supervision, funding acquisition, investigation, writing – original draft preparation, visualization, review and editing.

Conflicts of interest

There are no conflicts to declare.

Acknowledgements

Notes and references

1 Y. Duan, W. Wei, F. Xiao, Y. Xi, S.-L. Chen, J.-L. Wang, Y. Xu and C. Hua, High-valent cationic metal–organic macrocycles as novel supports for immobilization and enhancement of activity of polyoxometalate catalysts, *Catal. Sci. Technol.*, 2016, **6**, 8540.

2 S. C. A. Sousa, I. Cabrita and A. C. Fernandes, High-valent oxo-molybdenum and oxo-rhenium complexes as efficient

catalysts for X–H (X = Si, B, P and H) bond activation and for organic reductions, *Chem. Soc. Rev.*, 2012, **41**, 5641.

3 W. R. Thiel, On the Way to a New Class of Catalysts—High-Valent Transition-Metal Complexes That Catalyze Reductions, *Angew. Chem., Int. Ed.*, 2003, **42**, 5390.

4 S. Kim, K.-B. Cho, Y.-M. Lee, J. Chen, S. Fukuzumi and W. Nam, Factors Controlling the Chemoselectivity in the Oxidation of Olefins by Nonheme Manganese(IV)-Oxo Complexes, *J. Am. Chem. Soc.*, 2016, **138**, 10654.

5 J. A. L. da Silva, J. J. R. F. da Silva and A. J. L. Pombeiro, Oxovanadium complexes in catalytic oxidations, *Coord. Chem. Rev.*, 2011, **255**, 2232.

6 R. R. Langeslay, D. M. Kaphan, C. L. Marshall, P. C. Stair, A. P. Sattelberger and M. Delferro, Catalytic Applications of Vanadium: A Mechanistic Perspective, *Chem. Rev.*, 2019, **119**, 2128.

7 J. C. Pessoa and M. R. Maurya, Vanadium Complexes Supported on Organic Polymers as Sustainable Systems for Catalytic Oxidations, *Inorg. Chim. Acta*, 2017, **455**, 415.

8 M. Sutradhar, M. V. Kirillova, M. F. C. G. da Silva, L. M. D. R. S. Martins and A. J. L. Pombeiro, A Hexanuclear Mixed-Valence Oxovanadium(IV,V) Complex as a Highly Efficient Alkane Oxidation Catalyst, *Inorg. Chem.*, 2012, **51**, 11229.

9 X. Xu, H. Wang, C.-H. Tan and X. Ye, Applications of Vanadium, Niobium, and Tantalum Complexes in Organic and Inorganic Synthesis, *ACS Org. Inorg. Au*, 2023, **3**, 74.

10 I. Gryca, K. Czerwińska, B. Machura, A. Chrobok, L. S. Shul'pina, M. L. Kuznetsov, D. S. Nesterov, Y. N. Kozlov, A. L. Pombeiro, I. A. Varyan and G. B. Shul'pin, High Catalytic Activity of Vanadium Complexes in Alkane Oxidations with Hydrogen Peroxide: An Effect of 8-Hydroxyquinoline Derivatives as Noninnocent Ligands, *Inorg. Chem.*, 2018, **57**, 1824.

11 D. Dragancea, N. Talmaci, S. Shova, G. Novitchi, D. Darvasiová, P. Rapta, M. Breza, M. Galanski, J. Kožíšek, N. M. R. Martins, L. M. D. R. S. Martins, A. J. L. Pombeiro and V. B. Arion, Vanadium(V) Complexes with Substituted 1,5-bis(2-hydroxybenzaldehyde)carbohydrazones and their Use As Catalyst Precursors in Oxidation of Cyclohexane, *Inorg. Chem.*, 2016, **55**, 9187.

12 G. B. Shul'pin and Y. N. Kozlov, Kinetics and mechanism of alkane hydroperoxidation with *tert*-butyl hydroperoxide catalysed by a vanadate anion, *Org. Biomol. Chem.*, 2003, **1**, 2303.

13 M. Sutradhar, L. M. D. R. S. Martins, T. Roy Barman, M. L. Kuznetsov, M. F. C. Guedes da Silva and A. J. L. Pombeiro, Vanadium complexes of different nuclearities in the catalytic oxidation of cyclohexane and cyclohexanol – an experimental and theoretical investigation, *New J. Chem.*, 2019, **43**, 17557.

14 M. R. Maurya, Probing the synthetic protocols and coordination chemistry of oxido-, dioxido-, oxidoperoxido-vanadium and related complexes of higher nuclearity, *Coord. Chem. Rev.*, 2019, **383**, 43.

15 R. Dinda, P. Sengupta, M. Sutradhar, T. C. W. Mak and S. Ghosh, Solution Study of a Structurally Characterized Monoalkoxo-Bound Monooxo-Vanadium(V) Complex: Spontaneous Generation of the Corresponding Oxobridged Divanadium(V,V) Complex and its Electroreduction to a Mixed-Valence Species in Solution, *Inorg. Chem.*, 2008, **47**, 5634.

16 M. Y. Enbo, W. Ying, L. Shutao, W. Yangguang, L. Wang and C. Hu, A novel chain-like binuclear vanadium(V) coordination polymer containing mixed ligands: hydrothermal synthesis and crystal structure of [{VO$_2$(2,2'-bipy)}$_2$(tp)]$_\infty$ (tp=terephthalate), *Inorg. Chim. Acta*, 2003, **344**, 257.

17 E. Kiss, A. Benyei and T. Kiss, VO(IV) complexes of 3-hydroxypicolinic acid: a solution study and the structure of a supramolecular assembly in the solid state, *Polyhedron*, 2003, **22**, 27.

18 X.-M. Zhang, M. Liang Tong, H. Kay Lee and X.-M. Chen, The First Noncluster Vanadium(IV) Coordination Polymers: Solvothermal Syntheses, Crystal Structure, and Ion Exchange, *J. Solid State Chem.*, 2001, **160**, 118.

19 K. Su, M. Wu, D. Yuan and M. Hong, Interconvertible vanadium-seamed hexameric pyrogallol[4]arene nanocapsules, *Nat. Commun.*, 2018, **9**, 4941.

20 S. P. Dash, A. K. Panda, S. Pasayat, R. Dinda, A. Biswas, E. R. T. Tiekink, S. Mukhopadhyay, S. K. Bhutia, W. Kaminsky and E. Sinn, *RSC Adv.*, 2015, **5**, 51852.

21 V. Vrdoljak, M. Mandarić, T. Hrenar, I. Đilović, J. Pisk, G. Pavlović, M. Cindrić and D. Agustin, Geometrically constrained molybdenum(VI) metallosupramolecular architectures: conventional Synthesis *versus* vapor and thermally induced solid-state structural transformations, *Cryst. Growth Des.*, 2019, **19**, 3000.

22 D. Cvijanović, J. Pisk, G. Pavlović, D. Šišak-Jung, D. Matković-Čalogović, M. Cindrić, D. Agustin and V. Vrdoljak, Discrete mononuclear and dinuclear compounds containing a MoO$_2$$^{2+}$ core and 4-aminobenzhydrazone ligands: synthesis, structure and organic-solvent-free epoxidation activity, *New J. Chem.*, 2019, **43**, 1791.

23 J. Pisk, M. Rubčić, D. Kuzman, M. Cindrić, D. Agustin and V. Vrdoljak, Molybdenum(VI) complexes of hemilabile aroylhydrazone ligands as efficient catalysts for greener cyclooctene epoxidation: an experimental and theoretical approach, *New J. Chem.*, 2019, **43**, 5531.

24 V. Vrdoljak, B. Prugovečki, D. Matković-Čalogović, R. Dreos, P. Siega and C. Tavagnacco, Zigzag Chain, Square Tetranuclear, and Polyoxometalate-Based Inorganic–Organic Hybrid Compounds - Molybdenum *vs.* Tungsten, *Cryst. Growth Des.*, 2010, **10**(3), 1373.

25 J. Pisk, D. Agustin and V. Vrdoljak, Tetranuclear molybdenum(VI) hydrazonato epoxidation (pre)catalysts: Is water always the best choice?, *Catal. Commun.*, 2020, **142**, 106027.

26 M. Mandarić, E. Topić, D. Agustin, J. Pisk and V. Vrdoljak, Preparative and Catalytic Properties of Mo^{VI} Mononuclear and Metallosupramolecular Coordination Assemblies Bearing Hydrazonato Ligands, *Int. J. Mol. Sci.*, 2024, **25**, 1503.

27 M. A. Fik, A. Gorczyński, M. Kubicki, Z. Hnatejko, A. Wadas, P. J. Kulesza, A. Lewińska, M. Giel-Pietraszuk, E. Wyszko and

V. Patroniak, New vanadium complexes with 6,6''-dimethyl-2,2':6',2''-terpyridine in terms of structure and biological properties, *Polyhedron*, 2015, **97**, 83.

28 M. Motevalli, D. Shah, S. A. A. Shah and A. C. Sullivan, A novel route to oxovanadium halides. Synthesis and X-ray structures of VOCl$_2$·3Py and VO$_2$Cl·2Py, *Polyhedron*, 1996, **15**, 2387.

29 E. Salojärvi, A. Peuronen, M. Lahtinen, H. Huhtinen, L. S. Vlasenko, M. Lastusaari and A. Lehtonen, Series of Near-IR-Absorbing Transition Metal Complexes with Redox Active Ligands, *Molecules*, 2020, **25**, 2531.

30 L. M. Mokry and C. J. Carrano, Steric control of vanadium(V) coordination geometry: a mononuclear structural model for transition-state-analog RNase inhibitors, *Inorg. Chem.*, 1993, **32**, 6119.

31 B. Baruah, S. P. Rath and A. Chakravorty, A Novel Pentacoordinated Dioxovanadium(V) Salicylaldiminate: Solvent Specific Crystallization of Dimorphs with Contrasting Coordination Geometries, Ligand Conformations and Supramolecular Architectures, *Eur. J. Inorg. Chem.*, 2004, **2004**, 1873.

32 P. I. d. S. Maia, V. M. Deflon, E. J. d. Souza, E. Garcia, G. F. d. Sousa, A. A. Batista, A. T. d. Figueiredo and E. Niquet, Biomimetic oxovanadium(IV) and (V) complexes with a tridentate (N,N,O)-donor hydrazonic ligand. Two X-ray crystal structure modifications of (2-acetylpyridine-benzoylhydrazonato)dioxovanadium(V), *Transition Met. Chem.*, 2005, **30**, 404.

33 M. R. P. Kurup, E. B. Seena and M. Kuriakose, Synthesis, spectral and structural studies of oxovanadium(IV/V) complexes derived from 2-hydroxyacetophenone-3-hydroxy-2-naphthoylhydrazone: polymorphs of oxovanadium(V) complex [VOL(OCH$_3$)], *Struct. Chem.*, 2010, **21**, 599.

34 Y. Jin and M. S. Lah, Polymorphism Driven by π–π Stacking and van der Waals Interactions: Preparation and Characterization of Polymorphic Vanadium Crystals of [V^{V}O(Hacshz)(OEt)] and [V^{IV}(Hacshz)$_2$], *Eur. J. Inorg. Chem.*, 2005, **2005**, 4944.

35 N. Heydari, R. Bikas, M. Shaterian, M. S. Krawczyk and T. Lis, Investigation of the substituent effects on the oxidation of styrene derivatives by silica-supported heterogeneous oxidovanadium(V) coordination compound, *Appl. Organomet. Chem.*, 2023, **37**, e6976.

36 M. Rubčić, D. Milić, G. Pavlović and M. Cindrić, Conformational Diversity of Thiosemicarbazonatovanadium(V) Complexes in the Solid State: From Polymorphism to Isostructurality, *Cryst. Growth Des.*, 2011, **11**, 5227.

37 T. Hu, Q. Wang, W. You, D. Song, C. Huang, Y. Xu and Z. Sun, Two new layered complexes supported by helical chains: Hydrothermal syntheses and crystal structures of [M(dpa)V$_2$O$_6$] (M = Zn(II) and Cu(II); dpa = 2,2'-dipyridylamine), *Inorg. Chem. Commun.*, 2008, **11**, 470.

38 J.-S. Qin, D.-Y. Du, S.-L. Li, Y.-Q. Lan, K.-Z. Shao and Z.-M. Su, pH-Tuned self-assembly of organic–inorganic hybrids based on different vanadate chains, Zn(II) ions and flexible

ligands: crystallizing in polar and centrosymmetric space group, *CrystEngComm*, 2011, **13**, 779.

39 A. Sukhikh, D. Bonegardt, D. Klyamer and T. Basova, Effect of non-peripheral fluorosubstitution on the structure of metal phthalocyanines and their films, *Dyes Pigm.*, 2021, **192**, 109442.

40 D. Klyamer, A. Sukhikh, D. Bonegardt, P. Krasnov, P. Popovetskiy and T. Basova, Thin Films of Chlorinated Vanadyl Phthalocyanines as Active Layers of Chemiresistive Sensors for the Detection of Ammonia, *Micromachines*, 2023, **14**, 1773.

41 Y. Horii, M. Makino, T. Yamamoto, S. Tatsumi, H. Suzuki, M. Noguchi, T. Yoshida, T. Kajiwara, Z.-Y. Li and M. Yamashita, Solid polymorphism and dynamic magnetic properties of a dodecylated vanadyl–porphyrinato complex: spin–lattice relaxations modulated by phase stabilisation, *Inorg. Chem. Front.*, 2022, **9**, 6271.

42 C. J. Brown, F. D. Toste, R. G. Bergman and K. N. Raymond, Supramolecular Catalysis in Metal–Ligand Cluster Hosts, *Chem. Rev.*, 2015, **115**, 3012.

43 C. Lescop, Coordination-Driven Syntheses of Compact Supramolecular Metallacycles toward Extended Metallo-organic Stacked Supramolecular Assemblies, *Acc. Chem. Res.*, 2017, **50**, 885.

44 B. H. Northrop, H.-B. Yang and P. J. Stang, Coordination-driven self-assembly of functionalized supramolecular metallacycles, *Chem. Commun.*, 2008, 5896.

45 T. R. Cook and P. J. Stang, Recent Developments in the Preparation and Chemistry of Metallacycles and Metallacages *via* Coordination, *Chem. Rev.*, 2015, **115**, 7001.

46 S. Leininger, B. Olenyuk and P. J. Stang, Self-assembly of discrete cyclic nanostructures mediated by transition metals, *Chem. Rev.*, 2000, **100**, 853.

47 B. H. Northrop, Y.-R. Zheng, K.-W. Chi and P. J. Stang, Self-Organization in Coordination-Driven Self-Assembly, *Acc. Chem. Res.*, 2009, **42**, 1554.

48 R. J. J. Jachuck, D. K. Selvaraj and R. S. Varma, Process intensification: oxidation of benzyl alcohol using a continuous isothermal reactor under microwave irradiation, *Green Chem.*, 2006, **8**, 29.

49 C. Ragupathi, J. J. Vijaya, S. Narayanan, S. K. Jesudoss and L. J. Kennedy, Highly selective oxidation of benzyl alcohol to benzaldehyde with hydrogen peroxide by cobalt aluminate catalysis: a comparison of conventional and microwave methods, *Ceram. Int.*, 2015, **41**, 2069.

50 A. Mahmood, G. E. Robinson and L. Powell, An improved oxidation of an alcohol using aqueous permanganate and phase-transfer catalyst, *Org. Process Res. Dev.*, 1999, **3**, 363.

51 A. L. Cánepa, V. R. Elías, V. M. Vaschetti, E. V. Sabre, G. A. Eimer and S. G. Casuscelli, Selective oxidation of benzyl alcohol through ecofriendly processes using mesoporous V-MCM-41, Fe-MCM-41 and Co-MCM41 materials, *Appl. Catal., A*, 2017, **545**, 72.

52 S. K. Hanson, R. T. Baker, J. C. Gordon, B. L. Scott, A. D. Sutton and D. L. Thorn, Aerobic oxidation of pinacol by vanadium (V) dipicolinate complexes: evidence for reduction to vanadium (III), *J. Am. Chem. Soc.*, 2008, **131**, 428.

53 V. R. Choudhary, A. Dhar, P. Jana, R. Jha and B. S. Uphade, A green process for chlorine-free benzaldehyde from the solvent-free oxidation of benzyl alcohol with molecular oxygen over a supported nano-size gold catalyst, *Green Chem.*, 2005, **7**, 768.

54 C. Xu, L. Zhang, Y. An, X. Wang, G. Xu, Y. Chen and L. Dai, Promotional synergistic effect of Sn doping into a novel bimetallic Sn-W oxides/graphene catalyst for selective oxidation of alcohols using aqueous H_2O_2 without additives, *Appl. Catal., A*, 2018, **558**, 26.

55 C. Kamonsatikul, T. Khamnaen, P. Phiriyawirut, S. Charoenchaidet and E. Somsook, Synergistic activities of magnetic iron-oxide nanoparticles and stabilizing ligands containing ferrocene moieties in selective oxidation of benzyl alcohol, *Catal. Commun.*, 2012, **26**, 1.

56 F. Shi, M. K. Tse, M.-M. Pohl, A. Brückner, S. Zhang and M. Beller, Tuning catalytic activity between homogeneous and heterogeneous catalysis: Improved activity and selectivity of free nano-Fe_2O_3 in selective oxidations, *Angew. Chem., Int. Ed.*, 2007, **46**, 8866.

57 V. Vrdoljak, B. Prugovečki, D. Matković-Čalogović, J. Pisk, R. Dreos and P. Siega, Supramolecular Hexagon and Chain Coordination Polymer Containing the MoO_2^{2+} Core: Structural Transformation in the Solid State, *Cryst. Growth Des.*, 2011, **11**, 1244.

58 J. Pisk, T. Hrenar, M. Rubčić, G. Pavlović, V. Damjanović, J. Lovrić, M. Cindrić and V. Vrdoljak, Comparative studies on conventional and solvent-free synthesis toward hydrazones: application of PXRD and chemometric data analysis in mechanochemical reaction monitoring, *CrystEngComm*, 2018, **20**, 1804.

59 G. H. Shahverdizadeh, S. W. Ng, E. R. T. Tiekink and B. Mirtamizdoust, *cis*-Dioxido[*N'*-(2-oxidobenzylidene) pyridinium-4-carbohydrazidato-κ^3*O,N',O'*]vanadium(V), *Acta Crystallogr., Sect. E: Struct. Rep. Online*, 2012, **68**, m236.

60 S. Y. Ebrahimipour, M. Mohamadi, I. Sheikhshoaie, S. Suárez, R. Baggio and M. Khaleghi, A novel oxido-vanadium(V) Schiff base complex: synthesis, spectral characterization, crystal structure, electrochemical evaluation, and biological activity, *Res. Chem. Intermed.*, 2016, **42**, 611.

61 Y.-H. Lu, Y.-W. Lu, C.-L. Wu, Q. Shao, X.-L. Chen and R. N. B. Bimbong, UV-visible spectroscopic study of the salicylaldehyde benzoylhydrazone and its cobalt complexes, *Spectrochim. Acta, Part A*, 2006, **65**, 695.

62 M. R. Maurya, S. Khurana, C. Schulzke and D. Rehder, Dioxo- and Oxovanadium(V) Complexes of Biomimetic Hydrazone ONO Donor Ligands: Synthesis, Characterisation, and Reactivity, *Eur. J. Inorg. Chem.*, 2001, **2001**, 779.

63 L. M. Martínez-Prieto, P. Palma, E. Álvarez and J. Cámpora, Nickel Pincer Complexes with Frequent Aliphatic Alkoxo Ligands [(^iPrPCP)Ni-OR] (R = Et, *n*Bu, *i*Pr, 2-hydroxyethyl). An Assessment of the Hydrolytic Stability of Nickel and Palladium Alkoxides, *Inorg. Chem.*, 2017, **56**(21), 13086.

64 S. R. Patra, S. Mondal, D. Sinha and K. K. Rajak, Mono *Versus* Dinuclear Vanadium(V) Complexes: Solvent Dependent Structural Versatility and Electro Syntheses of Mixed-Valence Oxovanadium(IV/V) Entities in Solution, *ACS Omega*, 2022, **7**, 11710.

65 M. Mandarić, B. Prugovečki, D. Cvijanović, J. Parlov Vuković, J. Lovrić, M. Skočibušić, R. Odžak, M. Cindrić and V. Vrdoljak, Vapour- and solvent-mediated crystalline transformations in Mo(VI) hydrazone complexes controlled by noncovalent interactions, *CrystEngComm*, 2019, **21**, 6281.

66 B. E. Bryant, W. C. Fernelius, D. H. Busch, R. C. Stoufer and W. Stratton, Vanadium(IV) Oxy(acetylacetonate), in *Inorganic Syntheses*, ed. T. Moeller, John Wiley & Sons, Inc, 1957, vol. 5, pp. 113–116.

67 O. Jović, T. Smolić, I. Primožič and T. Hrenar, Spectroscopic and Chemometric Analysis of Binary and Ternary Edible Oil Mixtures: Qualitative and Quantitative Study, *Anal. Chem.*, 2016, **88**, 4516.